Chinese Chemical Letters 35 (2024) 109463

Contents lists available at ScienceDirect

Chinese Chemical Letters

journal homepage: www.elsevier.com/locate/cclet

Colorimetric detection of α-glucosidase activity using Ni-CeO_2 nanorods and its application to potential natural inhibitor screening

Jia Chen[a,b], Yun Liu[b], Zerong Long[a], Yan Li[a,*], Hongdeng Qiu[b,*]

[a] Xinjiang Uygur Autonomous Product Quality Supervision and Inspection Institute, Urumqi 830000, China
[b] CAS Key Laboratory of Chemistry of Northwestern Plant Resources and Key Laboratory for Natural Medicine of Gansu Province, Lanzhou Institute of Chemical Physics, Chinese Academy of Sciences, Lanzhou 730000, China

ARTICLE INFO

Article history:
Received 12 November 2023
Revised 21 December 2023
Accepted 27 December 2023
Available online 29 December 2023

Keywords:
Ni-CeO_2
Ascorbic acid
α-Glucosidase
Inhibitor screening
Nanozyme

ABSTRACT

In this work, we established an exceptionally facile method for the preparation of Ni-CeO_2 nanorods in a kind of deep eutectic solvents (DESs) composed of L-proline and $Ce(NO_3)_3{\cdot}6H_2O$. First, Ni-CeO_2 nanorods were successfully prepared by adding $Ni(NO_3)_3{\cdot}6H_2O$ to DESs. Then, we found that Ni-CeO_2 nanorods prepared in DESs have more prominent oxidase-like activity than pure CeO_2. The outstanding catalytic activity of Ni-CeO_2 could be ascribed to its high Ce^{3+}/Ce^{4+} ratio. As a proof-of-concept application, the Ni-CeO_2 nanorods were successfully acted as a colorimetric platform for the sensitive determination of ascorbic acid and α-glucosidase activity, which displays excellent analytical performance. Moreover, this sensing platform was applied for screening natural α-glucosidase inhibitors, such as terpenoids from natural products. The results indicated that ursolic acid and oleanolic acid had good inhibitory rates. This strategy not only provides a new way to construct more kinds of nanomaterials from DESs, but also offers a facile and effective tool to screen the α-glucosidase natural inhibitors as potential anti-diabetic drugs.

Diabetes is one of the most common and complex diseases in the world. According to the data of the World Health Organization, there are more than 420 million people with diabetes worldwide [1]. Severe diabetes can lead to complications, such as diabetic retinopathy, cardiovascular disease, kidney disease and emotional disorders. α-Glucosidase (α-Glu) is a membrane binding enzyme located in the epithelium of the small intestine that can hydrolyze oligosaccharides/disaccharides into glucose and is considered to be one of the most critical targets for treating diabetes. The inhibitors of α-Glu can inhibit its enzyme activity, slow down the hydrolysis process of carbohydrates, and thus avoid an increase in postprandial blood sugar levels, so α-Glu inhibitors could be used to control blood sugar levels [2]. Many efforts have been made to search for inhibitors of α-Glu, including synthetic drugs (voglibose and miglitol) [3,4] and natural products (acarbose, luteolin, rutin, *etc.*) extracted from microorganisms and plants [5,6]. Natural inhibitors have better hypoglycemic effects, lower costs and fewer side effects than synthetic drugs [7]. Accordingly, the establishment of an effective strategy to detect α-Glu activity as well as screen natural α-Glu inhibitors is of great significance for the clinical treatment of diabetes.

Various nanomaterials have been used as nanozymes for the detection of biological enzymes (α-Glu [8], acid phosphatase [9,10], alkaline phosphatase [11–13], acetylcholinesterase [14], *etc.*). Metal oxide nanozymes have received special attention because of their acid-base and redox properties. Cerium(IV) oxide (CeO_2) nanozyme is one of the most widely used metal oxide catalysts. Similar to the catalytic cycle of natural oxidoreductases, CeO_2 nanozyme owns a mixed oxidation state of Ce^{4+} and Ce^{3+}, and displays high redox behavior by means of switching the two states [15]. However, the catalytic activity of CeO_2 still cannot meet the requirements of high affinity and detection sensitivity. Therefore, improving the catalytic activity of CeO_2 is important for developing high-performance nanozymes. According to the literature reports [16–19], doping metal ions into CeO_2 nanozymes is an effective way to regulate the surface, structure, and catalytic activity of pure CeO_2. The Cr^{3+}-doped CeO_2 (Cr-CeO_2) nanozymes [16] can increase the content of Ce^{3+} and make the activity of enzyme 3–5 times higher than that of pure CeO_2. Jampaiah *et al.* [17] found that Fe^{3+}-CeO_2 nanorods exhibited enhanced peroxidase-like activity. The doping of Pr increases the oxygen vacancy content in CeO_2 nanocubes, and greatly improves the affinity of the material

* Corresponding authors.
E-mail addresses: nhylsk001@163.com (Y. Li), hdqiu@licp.cas.cn (H. Qiu).

https://doi.org/10.1016/j.cclet.2023.109463
1001-8417/

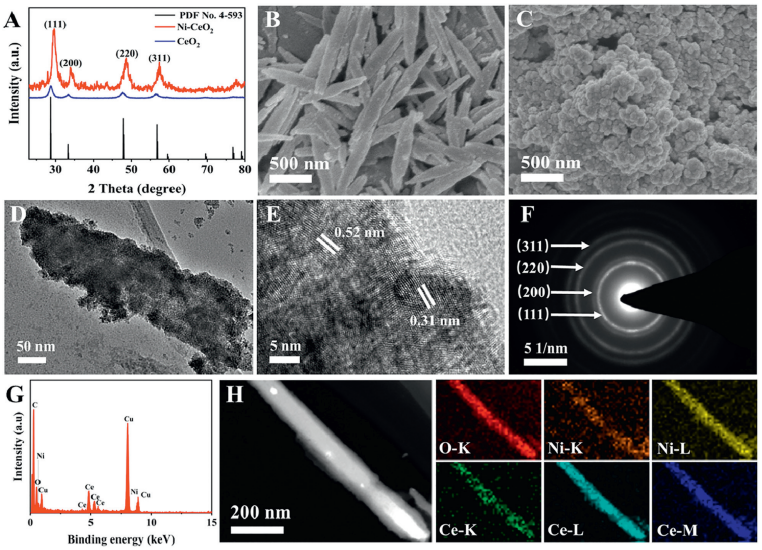

Fig. 1. (A) XRD of Ni-CeO_2 and pure CeO_2. SEM images of Ni-CeO_2 (B) and CeO_2 (C). (D) TEM, (E) HRTEM, (F) SAED, (G) EDX spectrum, (H) STEM-EDS mapping images of Ni-CeO_2.

to 3,3′,5,5′-tetramethylbenzidine (TMB) [18]. However, there is limited research on Ni doped CeO_2 (Ni-CeO_2) nanozymes [19]. As a new type of ionic liquid, deep eutectic solvents (DESs), can be used as reactants, solvents and templates [20], playing an enormous advantage in the morphology and crystallography of nanomaterials [21]. In our previous work [22], we demonstrated that nanomaterials prepared in DESs have better nanozyme properties than those prepared in water. Therefore, the study of metal-doped CeO_2 in DESs may provide a new way to prepare highly active nanozymes.

In this work, we developed Ni-doped CeO_2 nanorods with oxidase-like activity in DESs composed of L-Pro and $Ce(NO_3)_3 \cdot 6H_2O$. Based on the inhibitory effect of ascorbic acid (AA) on the color reaction of TMB catalyzed by Ni-CeO_2, 2-*O*-*α*-D-glucopyranosyl-L-ascorbic acid (AAG) was acted as substrate to construct a new approach for the colorimetric determination of *α*-Glu activity. When the activity of *α*-Glu was inhibited, the oxidation reaction of TMB resumed. Herein, acarbose was used as a control to screen three terpenoids (ursolic acid, uleanolic acid, glycyrrhetinic acid) isolated from natural products (Scheme 1). The results showed that ursolic acid and oleanolic acid had good inhibitory effects. The constructed colorimetric sensor platform is simple and cost-effective and is expected to become a simple method for screening inhibitors in natural products.

X-ray diffraction (XRD) was used to study the crystalline phase structure of Ni-CeO_2. The XRD pattern of Ni-CeO_2 is similar to the standard XRD pattern of CeO_2 (PDF No. 4-593) [23]. At the same time, we prepared pure CeO_2 under the same conditions, and its XRD pattern is consistent with the standard pattern (Fig. 1A). The diffraction peaks of (111), (200), (220) and (311) crystal planes can be found in Ni-CeO_2 and CeO_2, indicating that the crystallinity of the product is good. No peaks were found from other compounds such as $Ce(OH)CO_3$, NiO and $Ni(OH)_2$, indicating the feasibility of the method for preparing Ni-CeO_2. Compared with pure CeO_2, the XRD peaks of Ni-CeO_2 in Fig. 1A are slightly shifted to a lower angle [24], indicating that the successful incorporation of Ni^{2+} with smaller atomic radius into CeO_2 causes lattice distortion.

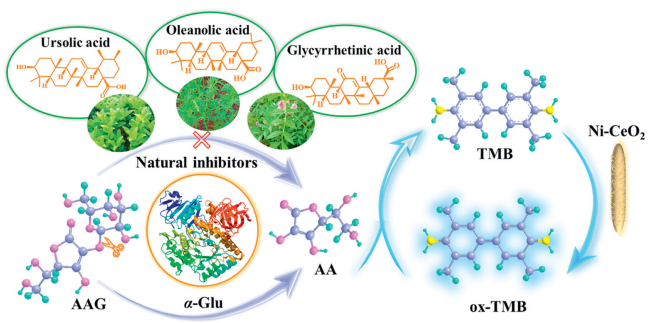

Scheme 1. Schematic diagram of the procedure for determining *α*-Glu activity and screening natural inhibitors.

The morphologies of Ni-CeO_2 and CeO_2 are displayed in Figs. 1B and C. Scanning electron microscopy (SEM) images show that Ni-CeO_2 is a nanorod, while CeO_2 is an aggregated particle. This indicates that $Ni(NO_3)_2 \cdot 6H_2O$ plays a certain role in the ordered growth of Ni-CeO_2, possibly because the presence of metal salts affects the hydrogen bonding in DESs. The structure and morphology of Ni-CeO_2 were further studied by TEM (Fig. 1D). The transmission electron microscopy (TEM) results are in good agreement with the SEM image. As shown in Fig. 1E, the (111) and (220) crystal surfaces of Ni-CeO_2 were observed by high resolution TEM (HRTEM). The crystal face spacing were 0.31 nm and 0.52 nm, respectively. The SAED image (Fig. 1F) exhibits a clear diffraction ring corresponding to the (311), (220), (200) and (111) crystal planes of CeO_2.

Energy dispersive X-ray (EDX) diagram (Fig. 1G) demonstrates the presence of the elements Ni and Ce. In addition, the element mapping (Fig. 1H) shows that Ni is doped into CeO_2, and that Ni and Ce are uniformly distributed. The Raman spectrogram in Fig. S1A (Supporting information) shows the characteristic peak of CeO_2 at 455 cm^{-1}. The TGA diagram shows that Ni-CeO_2 has good thermal stability up to 200 °C (Fig. S1B in Supporting information). When the temperature is less than 100 °C, the mass loss is the evaporation of water adsorbed on the Ni-CeO_2 surface. The mass loss curve decreases significantly in the temperature range of 200–244 °C, and the inflection point is about 214 °C. The total mass loss is approximately 22%. The results show that Ni^{2+} is inserted into the lattice of CeO_2, where DESs are the reactant, solvent and template for the formation of Ni-CeO_2 nanorods.

In order to further elucidate the composition of Ni-CeO_2 and the effect of doped Ni on the product, XPS testing was conducted on Ni-CeO_2 and CeO_2. In the full spectrum of Ni-CeO_2 (Fig. 2A), peaks of O 1s, Ce 3d, and Ni 2p could be observed, suggesting the presence of Ce, O, and Ni in our prepared material. The

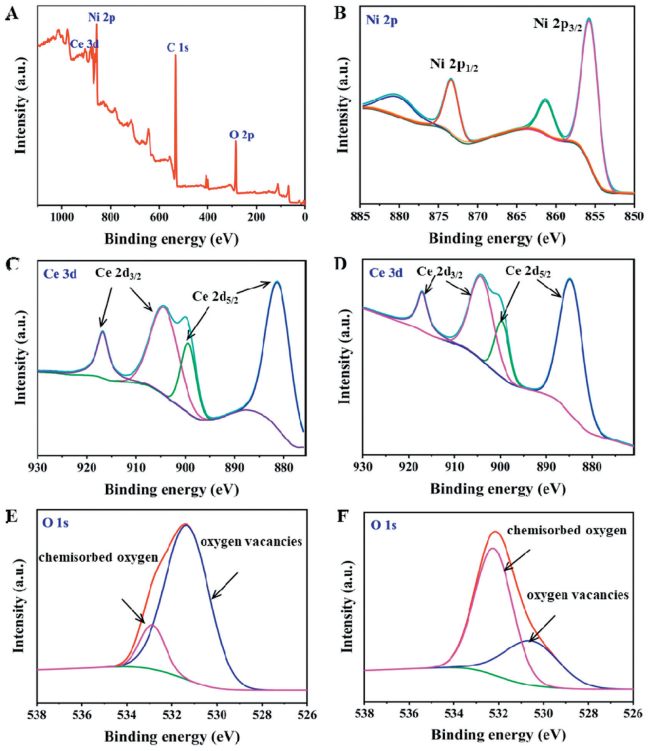

Fig. 2. (A) XPS spectrum of Ni-CeO_2. (B) Ni 2p XPS of Ni-CeO_2. Ce 3d XPS spectra of (C) Ni-CeO_2 and (D) CeO_2. O 1s XPS of (E) Ni-CeO_2 and (F) CeO_2.

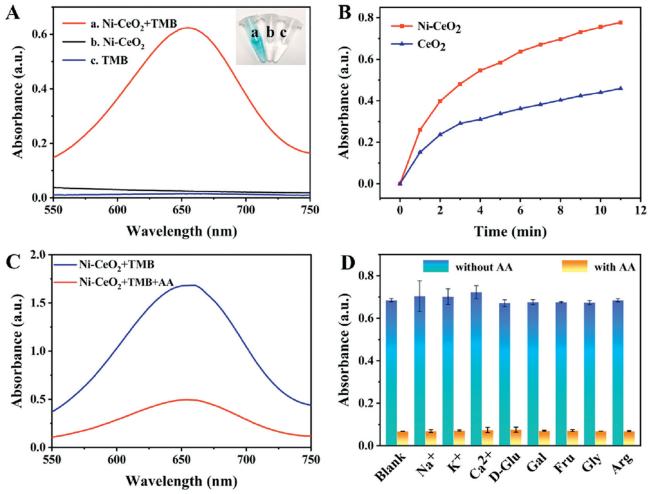

Fig. 3. (A) Absorption spectra of Ni-CeO_2+TMB, Ni-CeO_2, and TMB solutions. (B) The reaction rate of Ni-CeO_2 and CeO_2 over time. (C) Absorption spectra with and without AA in the Ni-CeO_2/TMB system. (D) The absorbance measured in the presence of other ions (200 mmol/L) and small molecules (20 mmol/L) with and without AA (20 mmol/L).

relative content of Ni and Ce in the product was determined by ICP-MS to be approximately 23:1. The two peaks located at 856 eV as well as 873 eV in Fig. 2B correspond to the binding energies of Ni $2p_{3/2}$ and Ni $2p_{1/2}$, respectively [24], proving the existence of Ni^{2+}. As depicted in Fig. 2C, in the Ce 3d spectrum of Ni-CeO_2, 916.8, 899.37, 904.2 and 881.2 eV correspond to Ce^{4+}(Ce $3d_{3/2}$, Ce $3d_{5/2}$) and Ce^{3+}(Ce $3d_{3/2}$, Ce $3d_{5/2}$) respectively [25], and the content of Ce^{3+} is 3.2 times that of Ce^{4+}. The content of Ce^{3+} in Ni-CeO_2 is significantly increased compared to that in CeO_2 (Ce^{3+}/Ce^{4+}= 0.27) (Fig. 2D), indicating that the addition of Ni promotes an increase in the ratio of Ce^{3+} to Ce^{4+}. As displayed in Figs. 2E and F, the oxygen vacancy to adsorbed oxygen ratios of Ni-CeO_2 and CeO_2 are 6 and 0.5, respectively. Compared with CeO_2 (Fig. 2F), Ni-CeO_2 (Fig. 2E) has more abundant oxygen vacancies, which is consistent with the conclusion of a high content of Ce^{3+} in Ni-CeO_2.

Of course, the factors affecting Ni-CeO_2 morphology, such as temperature, the amount of metal salt and reaction time were optimized in the experiment, and it was found that the material had the best morphology when the temperature was 80 °C, the amount of metal salt was 10 mmol/L, and the reaction time was 3 h (Figs. S2–S4 in Supporting information). Next, TMB was acted as the chromogenic substrate to investigate the oxidase-like activity of Ni-CeO_2. As illustrated in Fig. 3A, colorless TMB can be oxidized to oxidized TMB by Ni-CeO_2, the solution color turns blue, and the absorbance value at 652 nm increases significantly. As displayed in Fig. 3B, under the same conditions, the rate of TMB oxidation catalyzed by Ni-CeO_2 was approximately twice that of CeO_2, indicating that Ni doping plays an important role in enhancing the oxidase-like activity of CeO_2. Ni-CeO_2 exhibits better oxidase-like activity, which is attributed to the presence of Ni promoting the production of Ce^{3+}, resulting in a higher Ce^{3+}/Ce^{4+} ratio in the product [17].

In order to acquire the optimal oxidase-like activity of Ni-CeO_2, the influence of the concentration of Ni-CeO_2, the concentration of TMB, the pH value and the reaction temperature on the oxidase-like activity of Ni-CeO_2 was explored by means of the control variable method (Fig. S5 in Supporting information). The optimal Ni-CeO_2 concentration, TMB concentration, pH value and reaction temperature were 2 mg/mL, 10 mmol/L, 4.0, and 25 °C, respectively.

In addition, to further understand the oxidase-like properties of Ni-CeO_2, the steady-state kinetic parameters of TMB catalyzed by Ni-CeO_2 were also investigated. As seen in Fig. S6 in Supporting information, the K_m of Ni-CeO_2 obtained from the Lineweaver-Burk curve is 1.912 mmol/L, which is equivalent to or even smaller than the oxidase-like materials reported in the literature [26,27], indicating that Ni-CeO_2 has good binding ability to TMB.

AA, as an antioxidant and free radical scavenger, can effectively inhibit the TMB oxidation catalyzed by Ni-CeO_2. As can be seen from Fig. 3C, after injecting AA into the Ni-CeO_2/TMB system, the absorbance of the solution decreases sharply at 652 nm, indicating that this strategy is feasible for the detection of AA. Considering that the determination of AA may be interfered by other ions and small molecules, the effects of Na^+, K^+, Ca^{2+}, D-Glu, Gal, Fru, Gly-and Arg-on the detection system were studied. As presented in Fig. 3D, other metal ions and small molecules do not cause significant changes in absorbance values and do not interfere with the detection of AA. Thus, the analytical performance of Ni-CeO_2 for the determination of AA was investigated. It was clearly observed that the absorbance at 652 nm decreased with the increasing AA concentration (Fig. 4A), and a good linear relationship was obtained in the range of 2.0 μmol/L to 100 μmol/L between the change in absorbance and AA concentration (Fig. 4B). The LOD was computed to be 1.18 μmol/L. The analytical performance of the established methods is comparable to or superior to other reports (Table S1 in Supporting information) [9,28–35].

To assess the practicality and accuracy of our established method for AA in real samples, the detection of AA in human serum, urine and various fruit samples was further investigated. First, both human blood, urine and various juice samples from fresh fruits were centrifuged at 4500 rpm for 10 min and then the supernatants were collected, separately. The obtained human serum was diluted 5-fold, urine sample was diluted 50-fold, and various juice samples were diluted 100-fold. Subsequently, the standard addition methods were carried out. As listed in Table S2 (Supporting information), the initial content of AA in human

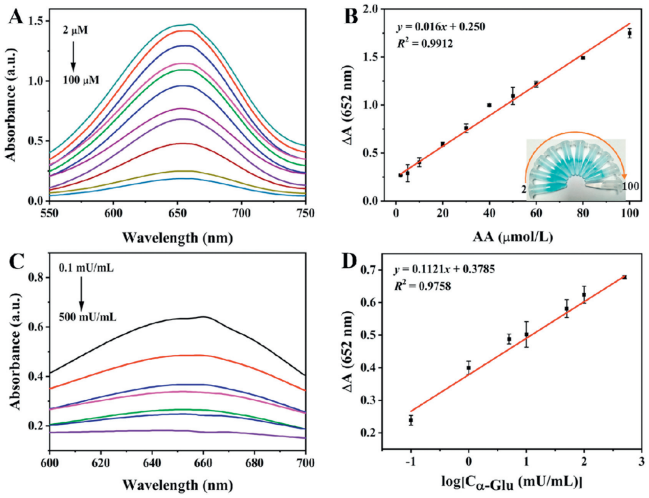

Fig. 4. (A) Absorption spectra of the Ni-CeO_2/TMB system with different concentrations of AA. (B) The linear relationship between AA concentration and ΔA at 652 nm ($\Delta A = A_0$ - A, where A_0 and A stand for the absorbance values of the solution at 652 nm in the absence and presence of AA, respectively). (C) Absorption spectra of the system with various α-Glu concentrations. (D) The linear relationship between ΔA and the log value of α-Glu activity. ($\Delta A = A_0$ - A, where A_0 and A represent the absorbance values of the solution at 652 nm in the absence and presence of α-Glu, respectively).

serum is approximately 33.51 μmol/L, and the detected AA in fresh lemons, navel oranges and grapes were 72.85, 32.36, and 17.23 μmol/L, respectively. The spiked experimental results show that the recoveries are in the range of 95.98%–105.3%, with relative standard deviations (RSDs) less than 4.30%, which proved that the potential applicability and accuracy of our established strategy for AA assay in real samples.

AA can be produced *via* α-Glu and AAG. Therefore, the proposed strategy, which sensitively responds to AA, can also be applied to measure the activity of α-Glu. As shown in Fig. S7 (Supporting information), AAG and α-Glu did not interfere with the detection system of Ni-CeO_2/TMB. When AAG and α-Glu exist simultaneously in the above system, AAG will be hydrolyzed to release AA, resulting in the reduction of oxidized TMB (ox-TMB) to TMB, with weakened absorbance at 652 nm [12]. Therefore, by means of measuring the absorbance reduction of the solution at 652 nm, the quantitative detection of α-Glu activity can be achieved. As illustrated in Fig. 4C, as the activity of α-Glu increased from 0.1 mU/mL to 500 mU/mL, the AA produced by α-Glu hydrolysis of AAG gradually increased, resulting in a gradual decrease in the maximum absorption value of the solution at 652 nm. Fig. 4D reveals that there is a good linear relationship between the change value of absorbance and the logarithm of the value of α-Glu activity with a detection limit of 0.050 mU/mL. The analytical performance of determining α-Glu activity in this work was better than that of many previously reported methods (Table S3 in Supporting information) [36–43].

Because α-Glu inhibitors are related to the treatment of type II diabetes, an increasing number of researchers have focused on the study of α-Glu inhibitors, especially to screen low-toxicity α-Glu inhibitors from natural products. Acarbose, a natural inhibitor provided by actinomycetes and a commercial antidiabetic drug [40], was used as a model analyte to investigate the approach's feasibility. As shown in Fig. S8A (Supporting information), acarbose does not affect the oxidase-like activity of Ni-CeO_2. When acarbose coexists with AAG and α-Glu, it can reduce ox-TMB reduction caused by the hydrolysis product AA of AAG, indicating that this strategy can be applied for screening α-Glu inhibitors. In order to further demonstrate the applicability of our proposed approach, the effects

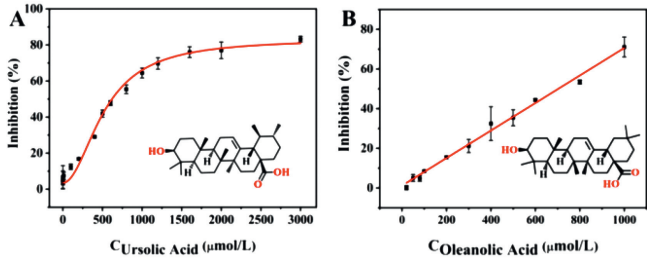

Fig. 5. Relationship between inhibition rate and concentration of (A) ursolic acid and (B) oleanolic acid.

of three terpenoids (ursolic acid, oleanolic acid and glycyrrhetinic acid) in ligustrum, glycyrrhetinic acid and glycyrrhetinic acid) on the activity of Ni-CeO_2 oxidase were investigated. As shown in Figs. S8B–D (Supporting information), ursolic acid, oleanolic acid and glycyrrhetinic acid did not interfere with the Ni-CeO_2/TMB detection system, proving that this colorimetric strategy can be used to screen α-Glu inhibitors from natural products.

Using 1 mmol/L acarbose as a control, the inhibitory effects of 1 mmol/L three terpenoids (ursolic acid, oleanolic acid, and glycyrrhetinic acid) on 100 μL of 100 mU/mL α-Glu were measured. The calculated inhibition rates are shown in Table S4 (Supporting information). Ursolic acid and oleanolic acid have better inhibitory effects, while glycyrrhetinic acid has weaker inhibitory effects. And the IC_{50} value of acarbose was 268 μmol/L (Fig. S9 in Supporting information), which was similar to the data reported in the literature [42], indicating the reliability of this strategy in screening inhibitors. In addition, the IC_{50} values of ursolic acid and oleanolic acid were 620 μmol/L and 702 μmol/L, respectively (Fig. 5).

In conclusion, we constructed a facile approach for the fabrication of Ni-CeO_2 nanorods in DESs composed of L-Pro and $Ce(NO_3)_3{\cdot}6H_2O$. It has been proven that Ni plays a crucial role in the morphology and catalytic properties of materials. The incorporation of Ni promotes the production of reduced Ce^{3+} and increases the proportion of Ce^{3+} and Ce^{4+} in the Ni-CeO_2 product. In addition, Ni-CeO_2 nanorods exhibit enhanced oxidase-like activity, which can achieve the assay of α-Glu activity and its natural inhibitor screening through colorimetric sensing. The results indicate that the synthesis strategy is simple and efficient, and can be further extended to the preparation of other transition metal-doped CeO_2. In addition, this constructed strategy also provides a convenient method to screen potential anti-diabetes drugs from natural products.

Declaration of competing interest

The authors declare that they have no known competing financial interests or personal relationships that could have appeared to influence the work reported in this paper.

Acknowledgments

This work was supported by the National Natural Science Foundation of China (No. 22374159), Regional Collaborative Innovation Project of Xinjiang (No. 2020E01051), CAS-JSPS Cooperation and Exchange Program (No. E20489GHZ1) and the Youth Innovation Promotion Association CAS (No. 2021420).

Supplementary materials

Supplementary material associated with this article can be found, in the online version, at doi:10.1016/j.cclet.2023.109463.

References

[1] H. Ki, H. Jang, J. Oh, et al., Anal. Chem. 92 (2020) 11530–11534.
[2] Y. Yao, X. Cheng, G. Ren, Food Funct. 5 (2014) 966–971.
[3] M.Z. Lin, W.M. Chai, Y.L. Zheng, Q. Huang, C. Ou Yang, Int. J. Biol. Macromol. 122 (2019) 1244–1252.
[4] U. Salar, M. Taha, K.M. Khan, et al., Eur. J. Med. Chem. 122 (2016) 196–204.
[5] L. Han, C. Fang, R. Zhu, et al., Int. J. Biol. Macromol. 95 (2017) 520–527.
[6] L. Jiang, Z. Wang, X. Wang, et al., RSC Adv. 10 (2020) 4529–4537.
[7] M. Mohiuddin, D. Arbain, A.K. Islam, M.S. Ahmad, M.N. Ahmad, Nanoscale Res. Lett. 11 (2016) 95.
[8] M. Shi, Y. Cen, G. Xu, et al., Anal. Chim. Acta 1077 (2019) 225–231.
[9] H. Wang, X. Wang, R.M. Kong, L. Xia, F. Qu, Chin. Chem. Lett. 32 (2021) 198–202.
[10] C. Chen, W. Liu, P. Ni, et al., ACS Appl. Mater. Interfaces 11 (2019) 47564–47570.
[11] S.B. He, P. Balasubramanian, A.L. Hu, et al., Sens. Actuators B: Chem. 321 (2020) 128511.
[12] C. Zhang, W. Liu, Z. Li, et al., ACS Sustain. Chem. Eng. 10 (2022) 1653–1663.
[13] X. Jiang, X. Wang, A. Lin, H. Wei, Anal. Chem. 93 (2021) 5954–5962.
[14] C. Zhang, P. Ni, B. Wang, et al., Chin. Chem. Lett. 33 (2022) 757–761.
[15] Z. Li, X. Yang, Y. Yang, et al., Chem. Eur. J. 24 (2018) 409–415.
[16] S. Zhang, Y. Liu, S. Sun, et al., Theranostics 11 (2021) 2806–2821.
[17] D. Jampaiah, T. Srinivasa Reddy, A.E. Kandjani, et al., J. Phys. Chem. B 4 (2016) 3874–3885.
[18] L. Jiang, S. Fernandez-Garcia, M. Tinoco, et al., ACS Appl. Mater. Interfaces 9 (2017) 18595–18608.
[19] W. Guo, M. Zhang, Z. Lou, et al., ChemCatChem 11 (2019) 737–743.
[20] X. Wei, J. Chen, M.C. Ali, J.C. Munyemana, H. Qiu, Microchim. Acta 187 (2020) 314.
[21] J.C. Munyemana, J. Chen, Y. Liu, Y. Wang, H. Qiu, ACS Sustain. Chem. Eng. 9 (2021) 15147–15156.
[22] Y. Liu, X. Wei, J. Chen, et al., Anal. Chem. 94 (2022) 5970–5979.
[23] C. Sun, J. Sun, G. Xiao, et al., J. Phys. Chem. B 110 (2006) 13445–13452.
[24] R. Murugan, G. Ravi, G. Vijayaprasath, et al., Phys. Chem. Chem. Phys. 19 (2017) 4396–4404.
[25] H. Xu, A.L. Wang, Y.X. Tong, G.R. Li, ACS Catal. 6 (2016) 5198–5206.
[26] L. Guo, K. Huang, H. Liu, J. Nanopart. Res. 18 (2016) 74.
[27] J. Wu, Z. Wang, X. Jin, et al., Adv. Mater. 33 (2021) 2005024.
[28] L. Luo, L. Huang, X. Liu, et al., Inorg. Chem. 58 (2019) 11382–11388.
[29] Z. Lou, S. Zhao, Q. Wang, H. Wei, Anal. Chem. 91 (2019) 15267–15274.
[30] G. Darabdhara, B. Sharma, M.R. Das, R. Boukherroub, S. Szunerits, Sens. Actuators B: Chem. 238 (2017) 842–851.
[31] P.K. Yadav, V.K. Singh, S. Chandra, et al., ACS Biomater. Sci. Eng. 5 (2019) 623–632.
[32] D. Guo, C. Li, G. Liu, X. Luo, F. Wu, ACS Sustain. Chem. Eng. 9 (2021) 5412–5421.
[33] C. Li, J. Zeng, D. Guo, et al., ACS Appl. Mater. Interfaces 13 (2021) 49453–49461.
[34] X. Zhou, Q. Qu, L. Wang, et al., J. Nanopart. Res. 22 (2020) 20.
[35] C.X. Chen, C.H. Zhang, P.J. Ni, et al., J. Anal. Test. 6 (2022) 67–75.
[36] J. Li, G. He, B. Wang, et al., Anal. Chim. Acta 1026 (2018) 140–146.
[37] A. Cao, Y. Tang, Y. Liu, ACS Appl. Mater. Interfaces 4 (2012) 3773–3778.
[38] C. Tang, Z. Qian, Y. Qian, et al., Sens. Actuators B: Chem. 245 (2017) 282–289.
[39] H. Chen, J. Zhang, H. Wu, K. Koh, Y. Yin, Anal. Chim. Acta 875 (2015) 92–98.
[40] H. Zhang, Z. Wang, X. Yang, et al., Anal. Chim. Acta 1080 (2019) 170–177.
[41] H. Ao, H. Feng, X. Huang, M. Zhao, Z. Qian, J. Mater. Chem. C 5 (2017) 2826–2832.
[42] S. Chen, Z. Li, W. Li, Z. Huang, Q. Jia, Biosens. Bioelectron. 82 (2021) 113198.
[43] M. Liang, G. Song, Y. Wan, et al., Chin. Chem. Lett. 35 (2024) 108573.